

A Multiwavelength Study of the Jets in FR-I Radio Galaxies: I. Data and Analysis *

Da-Min Meng and Hong-Yan Zhou

Center for Astrophysics, and Department of Astronomy and Applied Physics, University of Science and Technology of China, Hefei 230026; mdm@mail.ustc.edu.cn

Received 2005 April 26; accepted 2005 December 4

Abstract We compile a sample of 11 Fanaroff–Riley type I Radio Galaxies (FR-I RGs) with multi-wavelength observations to address the dynamic behavior of jets in these objects. Optical images acquired by the Hubble Space Telescope (HST) are carefully analyzed. The method and reduction procedure are described in detail. Unresolved optical cores emerge after having properly removed starlight from the host galaxies in eight of the FR-I RGs, of which five are new identifications. Broad band spectral properties of these newly identified compact cores are compared with that previously found in FR-I RGs, as well as the low-energy-peaked BL Lac objects. The similarity between them argues for the same non-thermal synchrotron origin. Well-resolved optical jets with knotty morphologies are found in three FR-I RGs in our sample, namely 3C 15, 3C 66B and B2 0755+37. The optical counterparts to the inner radio/X-ray jets are identified and a clear one-to-one correspondence between the optical, radio and X-ray knots is found. The structure and information on the optical jets are discussed. Physical parameters such as the knots position, flux and size are also presented. Detailed comparison between the multi-wavelength data and radiative and dynamic models of jet will be made in a forthcoming paper.

Key words: galaxies: active — galaxies: jets

1 INTRODUCTION

Radio galaxies often have radio jets which connect their active nuclei with their large radio lobes. Because of their association with the energy transfer processes in active galaxies and their close relation to the central engine, jets have been intensively studied since they were first discovered in extragalactic objects (Baade & Minkowski 1954). The number of known optical counterparts of radio jets in radio galaxies has been steadily increasing during the past years (e.g., Butcher et al. 1980; Keel 1988; Fraix-Burnet 1997; Kadler et al. 2003). Most of them were found by ground-based telescopes. With the increasing number of confirmed optical jets, some patterns in their properties begin to emerge. In the optical the jets commonly show knotty structures similar to that found in the radio (Biretta et al. 1991; Kataoka et al. 2003; Jackson et al. 1993). However, small differences between the optical and radio structures also exist in some objects (Sparks et al. 1996; Bai & Lee 2003; Marshall et al. 2002).

The apparent one-sidedness of the optical jets indicates that relativistic beaming plays an important role in modifying the distribution of the observed intensity. Sources with optical jets directed close to the line of sight should, on average, be smaller than the corresponding sources.

* Supported by the National Natural Science Foundation of China.

Sparks et al. (1995) studied the linear sizes of a sample of 3CR radio galaxies and found that the radio structures are smaller by a factor of ~ 3 in the galaxies with optical jets than in those without optical jets. This is in agreement with the relativistic beaming picture. However, intrinsic differences between the jet and counter jet cannot be ruled out completely (Fraix-Burnet 1997), and further research is required. Multiwavelength study of radio jets is essential since it can shed light on the kinematics of the jets. We have studied the broad band spectra of the knots in the jet of the well known RG, M87, and derived a conclusion that M87's jet is decelerated and slightly bend (Meng et al. 2005). Whether the kinematics of the jet in M87 is a common feature for FR-I RGs is intriguing. This motivates us to carry out a multiwavelength study of a sample of FR-I RGs.

Though radio jets have been observed in hundreds of FR-I RGs, optical and X-ray emission from the majority of these jets was virtually unknown until the end of the twentieth century due to lack of high resolution and high sensitivity observations in these bands. With the advent of the Chandra X-Ray Observatory, it became possible for the first time to study their X-ray properties in detail. Now, X-ray counterparts of radio jets have been identified in more than a dozen FR-I RGs (Harris & Krawczynski 2002, hereafter HK02), most of which were well resolved by Chandra. The HK02 sample serves as embarkation point for our present purpose. However, most objects in this sample are much further away than M87 and the jets in these RGs are in general intrinsically less powerful in the radio and the X-ray bands. Thus, if the broad band spectral energy distribution (SED) of their jets is similar to that of M87, the optical jets would be much fainter. Also, the high surface brightness part of the jets in these FR-I RGs is in general within a few arcseconds from the luminous nuclei and is fully contained within the luminous host galaxies. Optical imaging with high sensitivity and high spatial resolution is needed to detect such faint features in the steep gradients of starlight in elliptical galaxies. We note that jet emission is typically confined within a narrow region. The surface brightness of the jets in some sources could be high enough for detection at the spatial resolution of the Hubble Space Telescope (HST). The wide field view of the instrument WFPC2 on board HST and its low readout noise ($5e^-$) make it the best for identification of optical jets. In this paper we carry out a search for optical jets using archival HST/WFPC2 images of FR-I RGs in the HK02 sample and collect the multiwavelength data. We will compare in detail the multiwavelength data with radiative and dynamic models of jets in a forthcoming paper. The present paper is organized as follows: in the next section we describe in detail out procedure of analysing the HST/WFPC2 images. The results are presented in Section 3. A brief discussion and some straightforward implications are given in Section 4. Our preliminary conclusions are summarized in the last section.

2 HST OBSERVATIONS AND DATA ANALYSIS

2.1 HST Observations

A sample of 11 FRI-RGs with jets detected in the radio and in the X-ray were selected from HK02¹. We excluded M87 because its optical jet has been studied in detail by Perlman et al. (2001). We further excluded B2 0206+35, Cen A and 4C29.30, which have no WFPC2 observation. The objects in the sample often show jet-knots, hot-spots and/or radio lobes in the X-ray images and the radio images. It has been reported that optical jets (3C 31, 3C 66B, NGC 6251, Butcher et al. 1980; Keel 1988) and hot-spots (3C303, Meisenheimer et al. 1997) were detected in four sources by ground-based observations. The most recent list of optical jets was provided by Jester (2003)². The log of the WFPC2 images for each source is presented in Table 1.

Most of the radio galaxies in our sample with redshifts less than 0.1 were imaged with the PC chip on WFPC2 (the Wide Field and Planetary Camera 2) through F555W, F702W and F814W filters. M84 and 3C270 were also observed at other bandpasses. The projected spatial scale of PC chip is $0.0455'' \text{ pixel}^{-1}$ and the field of view $36'' \times 36''$. All the images were corrected for flat-fielding, bias and dark levels, and absolute sensitivity through the standard HST pipeline routines, and the final, calibrated images so produced were used. Subsequent reductions were carried out with the IRAF (NOAO Image Reduction and Analysis Facility) and STSDAS (space telescope science data

¹ The most updated list of X-ray jets can be found at <http://hea-www.harvard.edu/XJET/>.

² The full list of optical jets can be found online at <http://home.fnal.gov/jester/optjets/>.

Table 1 Journal of HST/WFPC2 observations for the sample of FR-I RGs

Object	R.A. (J2000)	Dec (J2000)	z	Filter	$\lambda_{\text{eff}}(\text{\AA})$	Date-Obs	Exposure (")
3C 15	00:37:02.23	-01:09:20.1	0.073	F555W	5443	1997 Feb 05	2×300
				F702W	6917	1995 June 18	2×140
3C 66B	02:23:08.86	+42:59:19.6	0.0215	F555W	5443	1999 Jan 31	2×230
				F702W	6917	1994 Mar 18	2×140
				F814W	7996	1999 Jan 31	2×230
3C31	01:07:25.96	+32:25:12.7	0.0169	F555W	5443	1998 Sept 23	2×230
				F814W	7996	1998 Sept 23	2×230
				F702W	6917	1995 Jan 19	2×140
B2 0755	07:58:25.74	+37:47:11.0	0.0428	F555W	5443	1999 May 19	300
				F814W	7996	1999 May 19	300
3C 303	14:42:59.74	+52:01:25.2	0.141	F555W	5443	1999 Sept 4	2×300
				F702W	6917	1994 Nov 19	2×140
NGC 6251	16:32:23.82	+82:32:43.6	0.0248	F555W	5443	1995 June 28	2×400
				F814W	7996	1995 June 28	2×260
				F814W	7996	1996 Sept 13	2×500
NGC 315	00:57:47.15	+30:20:48.5	0.0165	F555W	5443	1998 Feb 16	2×230
				F814W	7996	1995 Feb 16	2×230
3C 129	04:48:58.37	+45:01:58.0	0.0208	F555W	5443	1999 Mar 17	2×300
				F702W	6917	1994 Apr 20	300
M84	12:25:03.61	+12:53:13.1	0.0035	F547M	5483	1996 Mar 4	2×600
				F702W	6917	1994 Apr 4	2×140
				F814W	7996	1996 Mar 4	2×260
3C 296	14:16:54.61	+10:48:07.9	0.0237	F702W	6917	1994 Dec 14	2×140
3C 270	12:19:23.22	+05:49:29.6	0.0074	F547M	5483	1994 Dec 13	2×400
				F702W	6917	1994 May 3	2×140
				F675W	6717	1994 Dec 12	2×1000
				F791W	7881	1994 Dec 13	2×400

analysis system) software packages. The individual exposures of each source were combined with the CRREJ task of IRAF in order to remove cosmic-rays and to maximize the signal-to-noise (S/N) ratio.

2.2 Starlight Subtraction and Jet Measurement

Identification of optical jets and measurement of their optical fluxes require very accurate modelling and subtraction of the underlying starlight distribution. Following Meisenheimer et al. (1997), we fit ellipses to the isophotes at various major axis radii and take the whole family of ellipses yielded as the profile of the host galaxies. First we use the IMEXAM task in IRAF to estimate approximately the galaxy center, the ellipticity and position angle of isophote, then these parameters are fed into the task ISOPHOTE of the package ELLIPSE as initial values to produce a 1-dimensional intensity distribution of the underlying galaxy. During the isophotal modelling process, we let the ISOPHOTE task adjust the centroid, ellipticity and position angle of each ellipses, i.e., these geometric parameters of the galaxy are allowed to vary freely; and the length of the semi-major axis is increased by 10% in each step from the center to the outer region of the galaxy. Based on the output table of ELLIPSE, a model of the galaxy profile is created by the BMODEL task and then subtracted from the original image using the IMARITH task. The residual images have an average flux level close to zero, indicating that the starlight distribution has been successfully modelled and subtracted. A jet, if exists, can be readily isolated since any faint emission features can be easily detected on the residual images.

IRAF provides three methods for sampling of the image along the elliptical path at each iteration when fitting the isophotes: bi-linear interpolation, and either mean or median over elliptical annulus sectors. The method of bi-linear interpolation extracts a 1-pixel width sample from the image. When the distance between successive ellipses exceeds two pixels, many pixels will never be sampled. This may lose useful information in the image. The mean or median integration over

elliptical annuli can be used to overcome this problem and to extract all information from the image and no much difference between the result of them, thus we adopt the third method. In our analysis the sky background was modelled subtracted simultaneously with the starlight distribution. It should be pointed out that, however, if one wants to determine the true brightness profile of the host galaxy, the sky background, though very small, should be evaluated in regions far from the object and then subtracted from the whole image. This should be done before modelling the starlight distribution. Nevertheless, we note that modelling the galaxy without subtracting the background is already good enough for our purpose, which is to isolate the jet on the residual image.

The optical flux of the jets was measured from the residual image, which can be taken as free of contamination by the underlying starlight of the host galaxies and the sky background. This was done by summing the detected counts in a box with the same size as in the radio and the X-ray when the corresponding components detected in these two bands, and converted to flux density.

3 RESULTS

Optical emissions from unresolved core were detected in eight of the 11 FR-I RGs in our sample, three of which have been reported by Chiaberge et al. (1999). The high special resolution of HST images enables us to measure the optical emission from the individual components of the jets. The results are summarized in Table 2 and described in detail in this section.

3.1 Detected Optical Jets

Optical jets are clearly detected in three sources in our sample: 3C 15, 3C 66B and B2 0755+37. Their observed and starlight-subtracted images are displayed in Figures 1, 2 and 3, respectively. The profiles of count rate along the jet of the first two objects are shown in Figure 4. We did not create such a profile for B2 0755+37 due to the faintness and low S/N ratio of its optical jet. The following notes on each of the three source contain further explanatory details.

3C 15 is an unusual source with a radio morphology intermediate between FR-I and FR-II, and its radio power is larger than that of a number of classical FR-II RGs (Leahy et al. 1997). The optical jet has been identified in the HST images by Martel et al. (1998) and matches the radio jet very well. The integrated fluxes of the optical jet in *R*-band and *V*-band were presented by above authors. Thanks to the excellent spatial resolution of the HST ($\sim 0.1''$), the optical jet is fully resolved in directions along and perpendicular to its axis. Three prominent knots can be readily identified in the starlight-subtracted image (Fig. 1, right panel). We derived the flux density of each knot at 5.51×10^{14} Hz and 4.34×10^{14} Hz. The innermost knot (knot A) is broad and diffuse, extending $2.1'' - 2.8''$ from the nucleus. The second knot (knot B) lies at a projected distance of $3.1''$ from the nucleus. It is compact (FWHM $\sim 0.5''$) and well defined. The outermost knot, knot C locates at about $4.1''$ from the nucleus and it is also comparatively compact and well defined as knot B. The profile of count rate along the jet displayed in Figure 4 (left panel) is derived within a width of 11 pixels along the jet from the starlight-subtracted image at *V*-band.

3C 66B is a low-luminosity FR-I RG hosted by UGC1841. Its bright radio jet was first discovered by Northover (1973) and subsequently studied by many authors (e.g. Leahy, Jagers & Pooley 1986; Hardcastle et al. 1996). An X-ray jet extended up to $\sim 7''$ from the nucleus was clearly revealed by Chandra (Hardcastle et al. 2001). The optical jet in 3C 66B was first detected by Butcher et al. (1980) using ground-based telescope. The presence of five distinct knots along the jet with polarized optical emission was reported in a subsequent ground-based work (Fraix-Burnet, Nieto & Poulain 1989). The available HST/FOC images, including the F320W, F220W and F430W filters described by Macchetto et al. (1991) were of too low S/N ratio to enable a detailed study of the jet. This motivated us to search for the optical jet using the HST/WFPC2 images. Fortunately, an optical jet is readily evident in each of the three exposures at F814W, F555W, and F702W, after a careful removal of starlight contamination. The observed and starlight-subtracted images at F555W band are compared in Figure 2. The optical jet, indiscernible in the observed image, is obvious in the residual image, and is fully

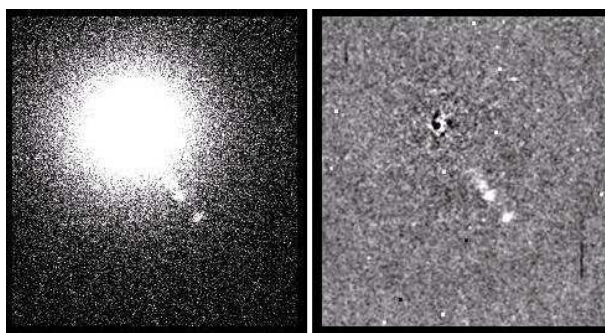


Fig. 1 Left: F555W (*V*-band) image of 3C15, with cosmic-rays removed. Right: Final residual image after subtracting the underlying galactic light and smoothing with a Gaussian of $\sigma = 1$ pixel. Figures are in the scale of $10.5'' \times 11.4''$. Orientation of the image is 115.5° .

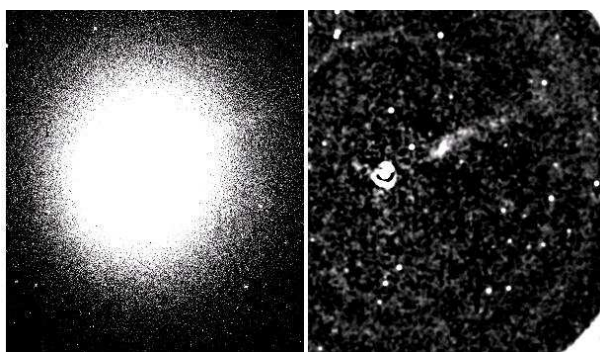


Fig. 2 Same as Figure 1 but for 3C66B. Figures are in the scale of $14.6'' \times 15.0''$. Orientation of the image is 116.5° .

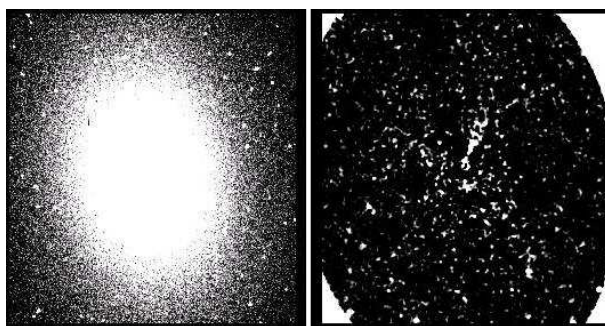


Fig. 3 Left: Original image of B2 0755+37 in *V*-band (F555W) and not removed cosmic-rays. Right: Final residual image after subtracting the underlying galactic light. To improve the visibility of jet features, a Gaussian smooth with $\sigma=3$ pixels was applied. Figures are on the scale of $11.4'' \times 12.3''$. Orientation of the image is 135.5° .

resolved parallel and perpendicular to its axis. The optical jet extends to $\sim 8''$ from the nucleus, beyond which it disappears into the noise. From the center the jet starts with a small structure labelled knot A, which is fainter and narrower than the next one, knot B. The jet becomes much brighter and reaches its highest brightness at knot B about $2.9''$ from the nucleus. It becomes broader and reaches a width of $\sim 0.7''$ at knot B. Further out are knots C, D and E. Beyond knot E, the jet gets too faint to be discernible. We made a comparison between the radio and the optical images and found an excellent correspondence in the positions of the knots in the two bands. The optical flux densities of the knots can be readily derived from the regions with well-defined knot positions and sizes.

Table 2 Broad Band Properties of the Jets in the Sample of FR-I RGs

Object	Dist. arcsec	$f_{\nu,5\text{ GHz}}$ mJy	$f_{\nu,5.51\text{ E}+14\text{ Hz}}$ $\mu\text{ Jy}$	$f_{\nu,4.34\text{ E}+14\text{ Hz}}$ $\mu\text{ Jy}$	$f_{\nu,3.75\text{ E}+14\text{ Hz}}$ $\mu\text{ Jy}$	$f_{\nu,1\text{ keV}}$ nJy	α_{ro}	α_{ox}
(1)	(2)	(3)	(4)	(5)	(6)	(7)	(8)	(9)
3C 15								
Core	0	43.5 ^{a(1)}	39.58	69.15		85.08 ⁽¹²⁾	0.61	1.04
A&B	2.1–3.1	72.9 ^a	3.72±0.54	4.92±0.86		1.77±0.41	0.88	1.2–1.3
knot C	4.1	37.5 ^a	1.34±0.21	1.58±0.29		1.29 ⁽¹²⁾	0.92	1.1–1.2
3C 66B								
Core	0	182.0 ⁽⁴⁾		78.6±1.1 ⁽⁴⁾		30±2.0 ⁽³⁾	0.68	1.24
knot A	1.4	2.72 ^{b(3)}	0.75±0.63	0.95±1.05	1.02±1.15	4.00 ⁽³⁾	0.73	0.86
knot B	2.9	25.1 ^{b(3)}	7.23±0.77	8.58±1.27	9.70±1.52	6.12 ⁽³⁾	0.73	1.16
knot C	4.5	7.39 ^{b(3)}	3.35±0.52	3.82±0.86	4.05±1.03	0.76 ⁽³⁾	0.69	1.36
knot D	5.7	9.78 ^{b(3)}	1.68±0.38	2.05±0.72	2.50±0.71	1.03 ⁽³⁾	0.77	1.22
knot E	7.8	13.7 ^{b(3)}	2.70±0.52	3.74±0.79	4.15±0.81	0.20 ⁽³⁾	0.76	1.56
M84								
Core	0	180.0 ⁽⁴⁾	42.1±1.0 ^{m(4)}		126±4.3 ⁽⁴⁾	23.31 ⁽⁵⁾	0.69	1.29
N2.5	2.5	3.50±0.6 ⁽⁵⁾	≤ 2.11 ^m	≤ 3.45	≤ 3.91	0.63±0.21 ⁽⁵⁾		
N3.3	3.3	13.0±3.0 ⁽⁵⁾	≤ 2.45 ^m	≤ 4.01	≤ 4.55	1.15±0.25 ⁽⁵⁾		
3C 129								
Core	0	51.85 ⁽¹⁰⁾	97.39	192.9		1.48 ⁽⁶⁾	0.54	1.84
N2.3	2.3	3.48 ^{c(10)}	≤ 5.70	≤ 12.0		0.83 ⁽⁶⁾		
N5.0	5.0	3.43 ^{c(10)}	≤ 3.61	≤ 12.2		0.36 ⁽⁶⁾		
3C 303								
Core	0	160.8 ^{d(11)}	57.52	137.3		237.8 ^{g(2)}	0.59	1.14
knot B	5.5	40.0 ^{d(2)}	≤ 9.38	≤ 8.43		0.45 ^{g(2)}		
knot C	9.0	40.0 ^{d(2)}	≤ 8.15	≤ 6.67		0.45 ^{g(2)}		
B2 0755								
Core		150±4 ^{e(7)}	48.42		75.93	47.6 ⁽⁷⁾	0.62	1.14
Jet	total	93±8 ^{e(7)}	4.36±1.50		5.41±2.20	9.70 ⁽⁷⁾	0.79	0.99
NGC 315								
Core	0	477±5 ⁽⁸⁾	12.95		38.64	40 ^{g(8)}	0.87	0.91
Jet	3–15	68.0 ⁽⁸⁾	≤ 5.33		≤ 9.46	4.30 ⁽⁸⁾		
3C 296								
Core	0	77 ⁽⁴⁾		5.42±0.48 ⁽⁴⁾		24.0 ⁽⁹⁾	0.84	0.86
NE	2.0–10	17.5 ^{f(9)}		≤ 4.59	1.90 ⁿ	1.2±0.3 ⁽⁹⁾	0.76	1.34

Note: — a, b, c, d, e, and f: radio flux density at 8.3, 8.2, 8.0, 1.5, 1.66, and 8.4 GHz; m, n, and h: optical flux density at 5.47×10^{14} , 1.3×10^{15} , 3.81×10^{14} Hz; g: X-ray flux density at 2 keV.

Ref. — (1) Leahy et al. (1997); (2) Kataoka et al. (2003a); (3) Hardcastle et al. (2001); (4) Chiaberge et al. (1999); (5) Harris et al. (2002); (6) X-ray count rates adopted from Harris & Krawczynski (2002) and converted to flux density in this paper; (7) Worrall et al. (2001); (8) Worrall et al. (2003); (9) Hardcastle et al. (2005); (10) Taylor et al. (2001); (11) Leahy & Perley (1991); (12) Kataoka et al. (2003b).

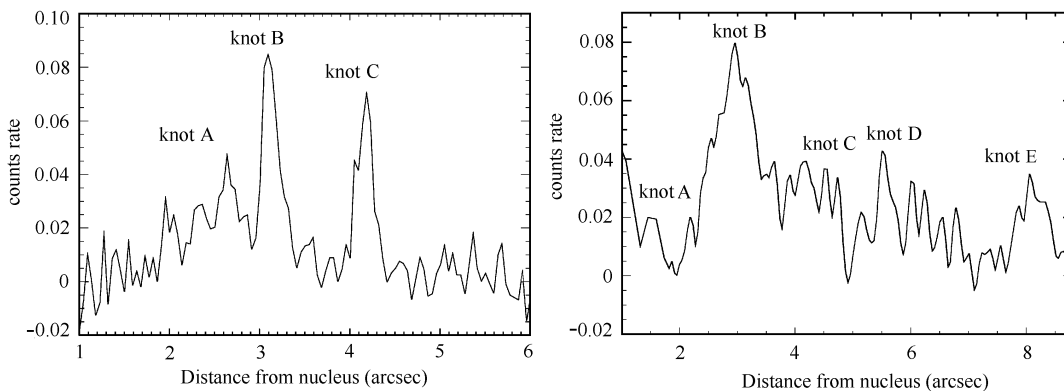


Fig. 4 Profile of the count rate in the F555W band along the jet for 3C 15 (left panel) and 3C 66B (right panel).

B2 0755+37 has a $4''$ long radio jet (Bondi et al. 2000) with an X-ray counterpart detected by Chandra (Worrall et al. 2001). Only two archival HST/WFPC2 exposures (F555W and F814W) were found for this source. Since there is only one exposure in each band, removal of cosmic rays cannot be performed using the previous method. We thus identify the cosmic ray events based on a comparison between the two band images. The cosmic rays were flagged individually with TEXT2MASK task in IRAF, and the pixels are excluded from the construction of the galaxy profile. After the subtraction of a galaxy elliptical model, a one-sided optical jet emerges, co-spatial with the South-East brighter radio jet. Here we calculated the jet flux for we may use it to build the continuum spectra for future study. The optical jet is very faint and the knot structure is not obvious. Only the total flux of the jet and the flux of the unresolved core are measured.

3.2 Non-detections

For three FR-I RGs in our sample optical jets have been detected in the ground-based observations, but they are not seen in the HST images. For these sources, $3\text{-}\sigma$ upper limits of the optical flux density of each component corresponding to that of the radio/X-ray jets were estimated and are presented in Table 2 (Col. (2): the distance of the knot from the nucleus. Cols. (3–7): the radio, optical, and X-ray flux density. Cols. (8) and (9): radio–optical and optical–X-ray spectral indices).

3C 31 High-resolution radio observation at 5 GHz was made and discussed by Burch (1977). A strong radio jet was seen to emerge from the nucleus at position angle 341° , decreasing in brightness with the distance from the nucleus. Evidence for an optical jet was claimed by Butcher et al. (1980) after subtracting a symmetric galaxy light by considering the effect of the dust lane which encircles the nucleus at a radius of about $3''$. However, the existence of an optical jet was questioned by later studies (Keel 1988; Fraix-Burnet et al. 1991). A dusty disk with diameter $\sim 7''$ along the major axis is present in its HST images. We use a mirror image about the galaxy’s major axis to generate a clean image free of any asymmetrical features, and subtract it from the original image. No significant optical emission aligned with radio jet was found in the residual image. We conclude that the optical jet of 3C 31, if exists, is too faint to be detected at the sensitivity of the present HST/WFPC2 observations.

NGC 6251 A prominent radio jet appears to the N-W (P.A. $\sim -66^\circ$) as well as a weak counter-jet on the opposite side of the nucleus (Perlay et al. 1984). The main jet is knotty. Optical emission from the jet region at $\sim 20''$ from the nucleus was claimed to be identified by ground-

based observation using the KPNO 2.1m telescope (Keel 1988). We cannot detect any optical emission associated with the inner radio jet due to the presence of an extended dusty disk which surrounds the nucleus. On the other hand, the first knot ($20''$) of the inner jet and the two radio knots ($4'$ and $6'$) of the outer jet are out of HST/WFPC2 field view, so we cannot even derive an upper limit of optical flux density for the jet in this object.

3C 303 is the only source with redshift ≥ 0.1 in our sample. Keel (1988) claimed an optical hotspot in their V -band image observed at the KPNO 2.1m telescope, which is coincident with the known radio hotspot. No clear detection of optical jet has been reported ever since. We did not find any evidence for the existence of an optical counterpart to the radio jet in the HST images. We derived an upper limit of flux density for knot B and knot C from our starlight-subtracted images.

For the remaining objects, no detection of optical jet has been reported in the literature, and we did not detect any optical jet either. The absence of a corresponding jet in the HST/WFPC2 images is not surprising: Assuming a typical value of optical to radio/X-ray flux density ratio, the optical flux density of jets in these sources is expected to be well below the background level on the PC chip images. We place an upper limit of optical flux density for each source which was also estimated from the residual images.

The radio and X-ray photometric data for the core and the jet (or components of the jet) were compiled from the literature and the results are also presented in Table 2. We visually compared the radio, optical and X-ray images and found excellent positional correspondence between the knots detected at these wavelengths. The only exception is 3C15. Though this source is well imaged in the radio at a resolution of $0''.34$ by Leahy et al. (1997), knot A and knot B are not resolved. We obtained the radio flux densities of knots A, B and C from the image of Leahy et al. (1997) by integration of the flux at 8.3 GHz in the regions defined by the optical/X-ray knots. Optical and X-ray flux density of knots A and B presented in Table 2 is the sum of the fluxes of the two knots.

4 DISCUSSION

It has been suggested that FR-I RGs might be misaligned counterparts of BL Lac objects (see Urry & Padovani 1995 for an extensive review, Mao et al. 2005). Direct comparison of the nuclear properties of FR-I RGs with BL Lacs is of vital importance to verify this unified scheme. Chiaberge et al. (1999) detected unresolved cores, the so-called CCCs (Central Compact Cores), in the majority of a complete sample of 33 FR-I RGs based on the HST observations in the optical. It was found that the optical flux of these CCCs is strongly correlated with the radio core. This correlation can be naturally interpreted as due to the radio and optical emissions having the same non-thermal synchrotron origin. As was mentioned in the last section, CCC was detected in nine of the 11 FR-I RGs in the present sample, out of which five were identified for the first time. The detection rate of CCC is similar to the sample of Chiaberge et al. (1999). We plot the optical flux of the newly identified CCCs against their core radio flux in Figure 5 (left panel). It can be seen that the FR-I RGs in the present sample are distributed around the correlation line defined by Chiaberge et al. (1999). This indicates that the nature of the unresolved optical cores in our FR-I RGs are the same as that of Chiaberge et al. (1999). Moreover, as it was suggested by these authors, the lack of broad lines in FR I RGs might be due to the lack of broad emission line regions (BLR) instead of dust obscuration (see Cao & Rawlings 2004 for an alternative interpretation). We present in Figure 5 (right panel) the α_{ro} vs. α_{ox} color-color diagram for the core emission of our FR-I RGs. The BL Lacs from the RGB (the ROSAT All-Sky-Green Bank) sample of Laurent-Muehleisen et al. (1999) are also plotted in this diagram for comparison. All but one (3C 129) are found in the region occupied by low-energy-peaked BL Lacs (LBLs). This result further supports the non-thermal synchrotron origin of the unresolved optical core, and the absence of a putative dusty torus in most, if not all, FR-I RGs.

The shape of the spectrum is very useful when examining the physics of the jets in FR-I RGs. In particular, spatially resolved broad band SED is a powerful tool in understanding the radiation process and the dynamics of jets. Meng et al. (2005) showed that in the nearby FR-I RG, M87, the jet decelerates as it propagates. We note that in 3C 66B the optical jet is well-resolved into four knots and in M87 the optical to X-ray spectral index α_{ox} of the knots increases with the

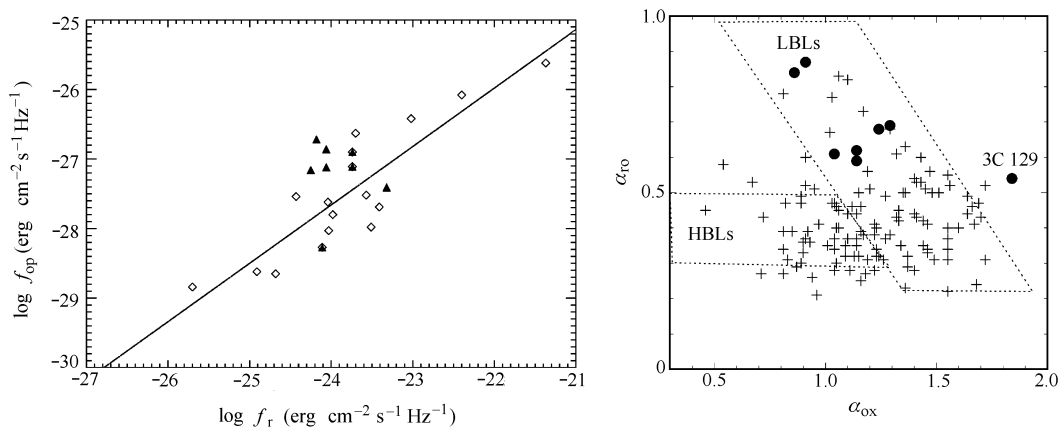


Fig. 5 Left: Plot of optical core flux vs. radio core flux for FR-I RGs. Diamonds denote objects from the sample of Chiaberge et al. (1999) and triangles denote our FR-I RGs. Dashed line is the best fit of Chiaberge et al. (1999). Right: An α_{ro} vs. α_{ox} color-color diagram for our FR-I RGs (filled circles) compared with RGB BL Lacs (cross) in the sample of Laurent-Muehleisen et al. (1999).

distance from the nucleus, while the radio to optical spectral index α_{ro} remains almost constant. This indicates that the two objects might have a similar kinematic behavior. Detailed comparison between the multi-wavelength data and radiative and dynamic models of the jet is beyond the scope of this paper. We postpone this to a future work.

5 SUMMARY

We have analyzed the HST/WFPC2 images of 11 FRI RGs mainly in three bands (F555W, F702W, and F814W). After the starlight contamination from the host galaxies was properly removed, eight of the sources showed an unresolved optical core, of which five are new identifications. The optical to radio flux ratios of these newly identified cores are similar to the values previously found in the FR-I RGs of Chiaberge et al. (1999), who showed convincing evidence for a non-thermal synchrotron origin of the central compact cores detected in the optical by HST. This is also supported by the similarity of broad band spectral indices of α_{ro} and α_{ox} between the cores in these FR-I RGs and low-energy-peaked BL Lacs. We find three FR-I RGs show clearly optical jets while optical emission can be seen in the regions previously occupied by radio and X-ray jets. Detailed structures of the jets are resolved at the sensitivity and resolution of HST. Optical flux density of the unresolved core and individual components of the jets have been extracted from the starlight-subtracted images with typical error of 10%–30%. A meaningful upper limit of flux density for the jet or its individual component was assigned when no obvious optical emission co-spatial with radio/X-ray jet was found. We found the spatially resolved spectral shapes of the jet in 3C 66B to be very similar to those in M87, indicating that the jet in 3C 66B might also be decelerating as it propagates, as was previously found in M87.

Acknowledgements We thank the anonymous referee for significant suggestions that lead to improvement of the paper. We also thank Hao, C. N. for her beneficial comments on image reduction and Prof. Wang, J. X. for his kind help about the usage of IRAF. Thanks are also due to P. Leahy and G. B. Taylor for letting us use their radio images. This work is supported by the NSFC through Grant 10233030, the Bairen Project of CAS, and the Key Program of Chinese Science and Technology Ministry.

References

- Baade W., Minkowski R., 1954, *ApJ*, 119, 215
Bai J. M., Lee M. G., 2003, *ApJ*, 585, L113
Biretta J. A., Stern C. P., Harris D. E., 1991, *AJ*, 101, 1632
Bondi M., Parma P., de Ruiter H. et al., 2000, *MNRAS*, 314, 11
Burch S. F., 1977, *MNRAS*, 181, 599
Butcher H. R., van Breugel W., Miley G. K., 1980, *ApJ*, 235, 749
Cao X., Rawlings S., 2004, *MNRAS*, 349, 1419
Chiaberge M., Capetti A., Celotti A., 1999, *A&A*, 349, 77
Ferrarese L., Pogge R. W., Peterson B. M. et al., 2001, *ApJ*, 555, L79
Fraix-Burnet D., 1997, *MNRAS*, 284, 911
Fraix-Burnet D., Golombek D., Macchetto F. D., 1991, *AJ*, 102, 562
Fraix-Burnet D., Nieto J. L., Poulain P., 1989, *A&A*, 221, 1
Hardcastle M. J., Birkinshaw M., Worrall D. M., 2001, *MNRAS*, 326, 1499
Hardcastle M. J., Alexander P., Pooley G. G., Riley J. M., 1996, *MNRAS*, 278, 273
Harris D. E., Krawczynski H., 2002, *ApJ*, 565, 244
Harris D. E., Finoguenov A., Bridle A. H. et al., 2002, *ApJ*, 580, 110
Jackson N., Sparks W. B., Miley G. K., Macchetto F., 1993, *A&A*, 269, 128
Jester S., 2003, *New Astronomy Reviews*, 47, 427J
Kadler M., Ros E., Kerp J. et al., 2003, *New Astronomy Review*, 47, 569
Kataoka J., Leahy J.P., Edwards P. G. et al., 2003a, *A&A*, 399, 91
Kataoka J., Leahy J.P., Edwards P. G. et al., 2003b, *A&A*, 410, 833
Keel W. C., 1988, *ApJ*, 329, 532
Kroberg P. P. et al., 1977, *APJ*, 218, 8
Leahy J. P., Jagers W. J., Pooley G. G., 1986, *A&A*, 156, 234
Leahy J. P., Black A. R. S., Dennett-Thorpe J. et al., 1997, *MNRAS*, 291, 20
Macchetto F., Albrecht R., Pooley C. et al., 1991, *ApJ*, 373, 55
Mao L. S., Xie G. Z., Bai J. M. et al., 2005, *ChJAA*, 5, 471
Martel A. R., Sparks W. B. et al., 1998, *ApJ*, 496, 203
Marshall H. L., Miller B. P. et al., 2002, *ApJ*, 564, 683
Meisenheimer K., Yates M. G., Roser H. J., 1997, *A&A*, 325, 57
Meng D. M., Wang C. C. et al., 2005, *Astronomical Research & Technology*, accepted
Nieto J. L., 1983, *MNRAS*, 203, 39p
Northover K. J. E., 1973, *MNRAS*, 165, 369
Perlay R. A., Bridle A. H., Willis A. G. et al., 1984, *ApJs*, 54, 291
Perlman E. S., Biretta J. A., Sparks W. B. et al., 2001, *ApJ*, 551, 206
Sparks W. B., Biretta J. A., Macchetto F., 1996, *ApJ*, 473, 254
Sparks W. B., Golombek D., Baum S. A. et al., 1995, *ApJ*, 450, L55
Worrall D. M., Birkinshaw M., Hardcastle M. J., 2001, *MNRAS*, 326, L7
Worrall D. M., Birkinshaw M., Hardcastle M. J., 2003, *MNRAS*, 343, 73